Spontaneous Formation of Zigzag Chains at the Metal-Insulator Transition in the β-Pyrochlore CsW_{2}O_{6}

Daigorou Hirai, Martin Bremholm, Jared M. Allred, Jason Krizan, Leslie M. Schoop, Qing Huang, Jing Tao, and R. J. Cava

Phys. Rev. Lett. **110**, 166402 — Published 16 April 2013

DOI: 10.1103/PhysRevLett.110.166402

Spontaneous Formation of Zigzag Chains at the Metal-Insulator Transition in the β-pyrochlore CsW_2O_6

Daigorou Hirai[1], Martin Bremholm[1+], Jared M. Allred[1++], Jason Krizan[1], Leslie M. Schoop[1], Qing Huang[2], Jing Tao[3] and R. J. Cava[1]

[1]Department of Chemistry, Princeton University, Princeton, New Jersey 08544, USA
[2]NIST Center for Neutron Research, National Institute of Standards and Technology, Gaithersburg, Maryland, 20899, USA
[3]Condensed Matter Physics and Materials Science Department, Brookhaven National Laboratory, Upton, New York 11973, USA

A paramagnetic metal to non-magnetic insulator transition at T_{MIT} = 210 K is reported for the ß-pyrochlore oxide CsW_2O_6, accompanied by a first order structural transition that creates <110> oriented chains in the pyrochlore lattice. Comparison of CsW_2O_6, which has 1 electron per 2 W sites, to the fully d^0 analog $CsTaWO_6$ shows that the transitions are electronically driven. Co-refinement of high resolution synchrotron X-ray and neutron diffraction data shows that the structural distortion that creates the W chains cannot be attributed to simple charge or orbital ordering. DFT calculations suggest that the phase transition is driven by a sharply peaked electronic density of states near the Fermi energy in the cubic ß-pyrochlore phase. A further electronic instability is required to create the insulating ground state.

[+]present address: Center for Materials Crystallography, Department of Chemistry and iNANO, Aarhus University, Aarhus C, DK-8000, Denmark.
[++]present address: Argonne National Laboratory, 9700 S. Cass Avenue Argonne, Illinois, 60439, USA

Geometric frustration, which arises when geometrical structural constraints promote competition between local states that are energetically degenerate, has been one of the most intensively studied subjects in condensed matter physics in recent years. A phase transition that lifts the degeneracy by lowering the local symmetry may be induced if the coupling of electronic and structural degrees of freedom is sufficiently strong. In pyrochlores ($A_2B_2O_7$) and spinels (AB_2O_4), the B ion sublattice consists of a three-dimensional network of corner sharing tetrahedra, known as the pyrochlore lattice, which underpins the strong geometrical frustration effects. When occupied by a non-integer number of electrons per site, simple charge order is suppressed and the eventual formation of a nontrivial charge state occurs. The $CuIr_2S_4$ and AlV_2O_4 spinels, for example, form complex Ir octamers [1] and V heptamers [2]. Some systems, however, maintain a uniform charge metallic state to low temperatures and exhibit ground states other than charge-ordering, such as heavy Fermion states (e.g. LiV_2O_4 [3]) or superconductivity (e.g. $A Os_2O_6$ (A = K, Rb, Cs) [4-8]).

CsW_2O_6 is a rare example of a mixed-valence pyrochlore oxide, with an average formal W valence of 5.5+, i.e. 1 electron per 2 W sites. It is a non-isoelectronic analogue to the intensively studied $A Os_2O_6$ (A = K, Rb, Cs) superconductors. CsW_2O_6 crystallizes in the ß-pyrochlore type structure at room temperature [9]. The existence of a phase transition at 215 K has been described in a preliminary report [10]. In this Letter, we report a metal-insulator transition (MIT) accompanied by a structural transition in CsW_2O_6 at 210 K. We find the formation of W zigzag chains below this transition. The structural distortion cannot be attributed to a simple charge ordered or orbitally ordered state, though the symmetry of the conducting lattice has clearly decreased and resulted in chain formation. Electronic structure calculations show the presence of a high density of states (DOS) near the Fermi energy (E_F) in the cubic ß-pyrochlore phase that is strongly suppressed at the transition. CsW_2O_6 therefore appears to be a unique example of a MIT accompanied by a complex structural transition on the pyrochlore lattice.

Polycrystalline CsW_2O_6 samples were prepared as described in ref. [9]. Washing in distilled water removed excess Cs_2WO_4. Synchrotron powder X-ray diffraction (SXRD) measurements were conducted from 100 K to 400 K in 20 K steps at beamline 11-BM at the Advanced Photon Source (Argonne

National Laboratory), with wavelength λ = 0.413115 Å, and neutron powder diffraction data were recorded using the BT1 spectrometer at the NIST Center for Neutron Research with wavelengths λ = 1.540 and 2.078 Å. Electron diffraction was carried out in a JEOL 3000F transmission electron microscope equipped with a Gatan liquid-helium cooling stage. Crystal structures were refined by the Rietveld method using the FULLPROF program. [11] Magnetic susceptibility, resistivity and specific-heat measurements were performed by using MPMS and PPMS (Magnetic and Physical Properties Measurement System, Quantum Design) instruments. Resistivity measurements were performed on synthesized, washed powders pressed into pellets and fired at 500 °C. The pellets were not dense, but higher temperature sintering is not possible due to the instability of the phase at high temperatures [9].

The synchrotron X-ray and neutron diffraction patterns of CsW_2O_6 at room-temperature are all consistent with the previously reported cubic ß-pyrochlore structure with space group $Fd\bar{3}m$ [9]. The refinement of this model gave good fits to the data (Supplemental Material [12]). No deviation from the ideal stoichiometric composition was observed.

Clear anomalies indicative of a phase transition were observed in the electrical resistivity, magnetic susceptibility, and specific-heat of CsW_2O_6 (Fig. 1). The resistivity of the high temperature phase above 210 K increases slightly on cooling, while exhibiting a remarkable increase below the transition, by as much as 5 orders of magnitude on cooling from 210 K to 60 K (Fig. 1a). The measured value of the resistivity at room-temperature (~ 1 Ωcm) is too high for a metal. The intrinsic transport property of CsW_2O_6 is considered to be metallic at room temperature with the high resistance of the samples originating from surface oxidation of the powders during processing (e.g. when washing in water). The fact that the room temperature resistivity continuously increases for samples exposed to air supports this conclusion. The possibility of small-polaron conduction, such as is observed in Fe_3O_4 [13] in its cubic spinel phase cannot be ruled out; thus further study is required to confirm the nature of the high temperature phase. The inset of Fig. 1a shows that the resistivity $\rho(T)$ below the transition follows the Arrhenius-type temperature dependence, $\rho(T) = A\exp(E_a/k_BT)$, where k_B is the Boltzmann constant. The fitting from 180 to 70 K gives a thermal activation energy of E_a

= 0.092 eV, indicating the opening of a charge gap. Thus, CsW_2O_6 undergoes a MIT on cooling below 210 K.

The magnetic susceptibility above the MIT, $\chi(T) \sim 1.0\times10^{-4}$ emu/mol, is comparable to or smaller than those reported for the metallic ß-pyrochlores $A Os_2O_6$ (A = Cs, Rb, K) [14], and can be ascribed to the Pauli paramagnetic susceptibility of a metal. Where the resistivity shows a marked change in slope at 210 K, the magnetic susceptibility shows an abrupt drop from a positive value to negative value (Fig. 1b), implying the formation of spin-singlets. A clear thermal hysteresis in the magnetic susceptibility data at the transition (inset, Fig. 1b) indicates that the transition is first order. The low temperature insulating phase exhibits a nearly temperature independent susceptibility, except for an upturn at low temperatures that can be attributed to a minor magnetic impurity with a small Curie constant of 1.6×10^{-3} emu/mol K. After considering a finite contribution from core diamagnetism, the negative susceptibility at low temperatures is too small to be due to an antiferromagnetic state of local moments.

The MIT in CsW_2O_6 is also clearly observed as a large jump in the specific-heat, as shown in Fig. 1c. This large jump is sharply in contrast with what is observed for the fully d^0 analogue $CsTaWO_6$ (inset to Fig. 1c) which does not exhibit a phase transition [15]. The difference between them clearly indicates that the phase transition in CsW_2O_6 is driven by an electronic instability due to the presence of 1 electron per two W sites. The specific-heat data around the MIT allows for an estimation of the change of entropy of ΔS = 3.7 J/mol K associated with the transition. Such a large entropy change is indicative of a drastic electronic transition with strong coupling to a lattice distortion. The other striking feature of the specific-heat in CsW_2O_6 is its large weight at low temperatures. This originates from the characteristic rattling of Cs atoms in the cage of the ß-pyrochlore structure. As shown in Fig. 1c, the specific-heat is well fitted by the same method adopted previously for ß-pyrochlore oxides. [14,16] The absence of a T-linear term in $C(T)$ indicates the absence of a significant electronic contribution to the specific-heat at low temperatures and therefore reflects the presence of a fully opened energy gap in the low temperature phase.

To investigate the structure of the insulating phase below T_{MIT}, high-resolution SXRD, powder neutron diffraction, and electron diffraction data were collected at various temperatures. Below the MIT (~210 K), weak

forbidden reflections in addition to those allowed in the $Fd\bar{3}m$ space group were seen in electron diffraction patterns (see Fig. 2c). These forbidden reflections were also observed in the SXRD patterns below T_{MIT} as many low intensity peaks, as shown in Fig. 2a. In addition, slight peak broadenings, suggestive of lowering of the crystal symmetry from cubic, were observed in the low temperature SXRD patterns. Quantitative structure refinements at 100 K involve co-refinement of both X-ray and neutron diffraction data to best determine both the W and O positions to high precision. The structure of the low temperature phase of CsW_2O_6 is found to be one of the known variations of ß-pyrochlore fluorides. These fluorides possess symmetries that are subgroups of the archetype cubic pyrochlore $Fd\bar{3}m$ and, in addition, are found in one single branch of the group-subgroup tree ($Fd\bar{3}m - I4_1/amd$ – $Imma$ – $Pnma$). [17] The superlattice peaks observed for low temperature CsW_2O_6 violate the extinction rules for the cubic face-centered subgroup and tetragonal/orthorhombic body-centered subgroups. All the superlattice reflections that are present in both the X-ray and neutron data collected at 100 K can be indexed on the primitive orthorhombic unit cell of space group *Pnma*. The relation between the cubic and orthorhombic cells is $\sqrt{2}a_o \approx \sqrt{2}b_o \approx a_c$ and $c_o \approx a_c$ (Fig. 3b). The intensity of the superlattice reflections observed in the X-ray diffraction data is ~ 10^{-3} of the fundamental reflections, which implies that the displacements of heavy elements W and Cs are very small through the MIT. The model for the low temperature orthorhombic *Pnma* phase was obtained by starting with the ideal pyrochlore positions. Parts of the Rietveld refinement plots for the SXRD and neutron data are shown in Fig. 2a. The refined *Pnma* model gives excellent fits to both the SXRD (also see Supplemental Material [12]) and neutron diffraction data, and no magnetic diffraction peaks were observed below the MIT in the neutron diffraction data. A strong coupling of the structure to the MIT is observed in the temperature dependence of the SXRD data (Fig. 2b); the lattice parameters and the integrated intensity of a representative superlattice peak are shown to change discontinuously on cooling through the transition.

A close examination of the low temperature structure reveals that the structural transition involves significant though complex changes in the local structure. In contrast to the high temperature structure with a single W site, the W ions in the low-temperature structure are distributed in an

ordered way over two symmetry-independent positions in a 1:1 ratio. The resulting independent W1 and W2 atoms are arranged in chains along the orthorhombic *a* and *b* axes, respectively (Fig. 3a). The single W-O bond distance of 1.9314(4) Å for all tungsten atoms above the MIT is split into different sets of distances for W1 and W2 [18] below the transition. The most important first order electro-structural characteristic, the average W-O bond length, is virtually the same for both types of W below the transition: for W1 it is 1.932(5) Å and for W2 it is 1.929(7) Å. These differ by only 0.003 Å, and therefore W^{5+}-W^{6+} charge ordering does not drive the MIT and the spontaneous chain formation. Second-order bonding effects such as the mean square deviation (Δ^2) [19] from an ideal octahedral coordination have to be considered to see a difference between the sites. In the low temperature structure, $\Delta^2 = 0.0184$ and 0.0687 for W1 and W2, respectively. Even at this level, however, there is no clear indication of charge ordering in the sites - both W1 and W2 are in much more regular octahedra than are found for $5d^0$ W^{6+} in WO_3, $\Delta^2 = 0.714$ and 0.659 [20], and much closer to what is found for the uniform charge state in the hexagonal tungsten bronze $Rb_{0.33}WO_3$, where $\Delta^2 = 0.119$ and 0.088 [21]. Further there is no clear indication of orbital ordering of partially occupied $5d$ orbitals within the chains below the phase transition.

Thus the structural transition in CsW_2O_6 at the MIT is more complex than can be explained by simple charge or orbital ordering. Non-magnetic, insulating ground states in systems with the pyrochlore lattice have also been observed, for example, in $Tl_2Ru_2O_7$ [22], $CuIr_2S_4$ [1], $MgTi_2O_4$ [23] and $LiRh_2O_4$ [24]. In $CuIr_2S_4$ and $MgTi_2O_4$, orbital orderings result in short transition-metal bonds forming spin-singlets. In contrast, there is no signature of dimer formation in CsW_2O_6. The W-W distances within the W1 and W2 chains are uniform and within 0.001 Å of each other (3.649 and 3.650 Å respectively). There has, however, been a significant differentiation of the interchain W1-W2 separations to longer (3.701 Å) and shorter (3.598 Å) distances, forming zigzag chains in the structure (Fig. 3c). This 0.1 Å differentiation of distances is the largest by far in the structure and is its primary response to the electronic instability. The same type of Ru^{4+} ($4d^4$, S= 1) zigzag chain in Tl_2RuO_7 is considered to be a Haldane chain which is responsible for its non-magnetic ground state at low temperature. [22] However, this cannot be the case for CsW_2O_6 where only one electron

occupies two W sites.

Strong coupling between electronic and structural degrees of freedom is rare in 5*d*-based transition metal compounds due to the diffuse character of the 5*d* orbitals. For pyrochlore oxides, however, the strong deviation of the M-O-M bond angles from 180 degrees results in relatively poor overlap of metal-5*d* and oxygen-2*p* orbitals and therefore the presence of narrower bands, for which such interactions are more normally seen. Indeed our electronic structure calculations [25], carried out for the high temperature phase, show evidence of electronic instability for cubic ß-pyrochlore CsW_2O_6. This phase has a high, sharply peaked DOS near E_F, as shown in Fig. 4, dominated by hybridized W 5*d* and O 2*p* states. The partially filled t_{2g} manifold of width 2.8 eV is consistent with the metallic phase above the MIT. The DOS shows relatively narrow features in energy. Similarly sharp features in the t_{2g} DOS have been reported for other pyrochlore lattice compounds such as $LiTi_2O_4$, LiV_2O_4 and KOs_2O_6, arising from dispersionless bands produced by geometrical frustration [26-28]. E_F of CsW_2O_6 is located near very sharp peaks in the DOS - the calculated DOS for CsW_2O_6 at E_F is $N(E_F)$ = 4.72 states/eV f.u., which is much larger than the $N(E_F)$ = 2.45 states/eV f.u. [29] for the related superconductor KOs_2O_6 with $Os^{5.5+}$ ($5d^{2.5}$). Fig. 4 shows that the structural change at the MIT significantly changes the electronic structure of CsW_2O_6 around E_F, where the sharply peaked character is dramatically suppressed and the DOS at E_F is reduced from 4.72 to 3.75 states/eV f.u. Note that our calculation for the low temperature phase has remnant states at E_F, and more ingredients, such as electronic correlations, appear to be required to elucidate the insulating ground state. This band instability inherent in the frustrated pyrochlore lattice of CsW_2O_6 at its electron count is likely the driving force for the MIT, though the resulting distortion of the lattice accompanying the transition cannot be described by any of the simple charge or orbital ordering schemes currently considered for pyrochlores.

In conclusion, we report a metal to non-magnetic insulator transition at T_{MIT} = 210 K in the ß-pyrochlore oxide CsW_2O_6. The low temperature crystal structure indicates the spontaneous formation of zigzag chains below the transition. Our electronic structure calculation for high temperature cubic phase exhibits sharp peaks of DOS in the t_{2g} manifold, which is related to the unique geometry of the pyrochlore lattice. Rather than leading to

superconductivity, as is seen in AOs$_2$O$_6$ (A = K, Rb and Cs), the high DOS at E_F in CsW$_2$O$_6$ gives rise to a band instability and results in a non-magnetic insulator ground state. The comparison between these compounds may lead to further understanding of the coupling of electronic and structural degrees of freedom in the pyrochlore lattice.

The authors thank B. H. Toby, L. Ribaud, and M. Suchomel at beamline 11-BM at the APS for their excellent diffraction data, and S. Jia for helpful discussions. This work was supported by the U.S. DOE Office of Basic Energy Sciences, Grant No. DE-FG02-45706. Use of the APS at Argonne National Laboratory was supported by the U. S. DOE, Office of Science, Office of Basic Energy Sciences, under Contract No. DE-AC02-06CH11357.

References

[1] P. G. Radaelli, Y. Horibe, M. J. Gutmann, H. Ishibashi, C. H. Chen, R. M. Ibberson, Y. Koyama, Y. S. Hor, V. Kiryukhin, and S. W. Cheong, Nature (London) **416**, 155 (2002).

[2] Y. Horibe, M. Shingu, K. Kurushima, H. Ishibashi, N. Ikeda, K. Kato, Y. Motome, N. Furukawa, S. Mori, and T. Katsufuji, Phys. Rev. Lett. **96,** 086406 (2006).

[3] C. Urano, M. Nohara, S. Kondo, F. Sakai, H. Takagi, T. Shiraki, and T. Okubo, Phys. Rev. Lett. **85,** 1052 (2000).

[4] S. Yonezawa, Y. Muraoka, Y. Matsushita, and Z. Hiroi, J. Phys.: Condens. Matter **16**, L9 (2004).

[5] S. Yonezawa, Y. Muraoka, Y. Matsushita, and Z. Hiroi, J. Phys. Soc. Jpn. **73**, 819 (2004).

[6] S. M. Kazakov, N. D. Zhigadlo, M. Brühwiler, B. Batlogg, and J. Karpinski, Supercond. Sci. Technol. **17**, 1169 (2004).

[7] M. Brühwiler, S. M. Kazakov, N. D. Zhigadlo, J. Karpinski, and B. Batlogg, Phys. Rev. B **70**, 020503(R) (2004).

[8] S. Yonezawa, Y. Muraoka, and Z. Hiroi, J. Phys. Soc. Jpn. **73**, 1655 (2004).

[9] R. J. Cava, R. S. Roth, T. Siegrist, B. Hessen, J. J. Krajewski and W. F. Peck, JR, J. Solid State Chem. **103**, 359 (1993).

[10] Y. Okamoto, Y. Nagao, M. Ichihara, J. Yamaura, and Z. Hiroi, presented at the Jpn. Phys. Soc. fall meeting, 22aQC-2 (2008).

[11] J. Rodriguez-Carvajal, Physica B **192**, 55 (1993).

[12] See Supplemental Material at (http://link.aps.org/supplemental/-------) for crystallographic parameters at 300 K and 100 K.

[13] D. Ihle, and B. Lorenz, J. Phys. C, Solid State Phys. **19**, 5239 (1986).

[14] Y. Nagao, J. Yamaura, H. Ogusu, Y. Okamoto, and Z. Hiroi, J. Phys. Soc. Jpn. **78**, 064702 (2009).

[15] A. V. Knyazev, N. G. Chernorukov, N. N. Smirnova, N. Yu. Kuznetsova, and A. V. Markin, Thermochimica Acta **470**, 47 (2008).

[16] The specific-heat was fitted by the following equation $C = C_E + aC_{D1} + (8\text{-}a)C_{D2}$, where C_E is contribution of Cs local mode represented by an Einstein oscillator and C_{D1} and C_{D2} are those of the W-O framework described by Debye phonons. The obtained parameters from the fitting are a = 1.98(6), Einstein temperature of Θ_E = 57.8(5) K, and Debye temperatures of Θ_{D1} = 224(4) K and Θ_{D2} = 767(7) K.

[17] K. Friese, J. Y. Gesland, and A. Grzechnik, Z. Kristallogr. **220**, 614 (2005).
[18] Obtained W-O bond lengths for low-temperature structure are as follows; W1-O: 1.925(6) Å × 2, 1.904(5) Å × 2, 1.967(5) Å × 2, W2-O: 1.876(12) Å, 2.005(11) Å 1.963(3) Å × 2, 1.882(5) Å × 2
[19] The mean square deviations from ideal octahedral symmetry (Δ^2) are calculated as $\Delta^2 = (1/6)\sum_{n=1,6}[(d_n - \langle d\rangle)/\langle d\rangle]^2 \times 100$, where $\langle d\rangle$ is average W-O bond length in a WO_6 octahedra.
[20] P. M. Woodward, A. W. Sleight, and T. Vogt, J. Phys. Chem. Solids **56**, 1305 (1995).
[21] R. Brusetti, P. Bordet, J. Bossy, H. Schober, and S. Eibl, Phys. Rev. B **76**, 174511 (2007).
[22] S. Lee, J. G. Park, D. T. Adroja, D. Khomski, S. Streltsov, K. A. McEwen, H. Sakai, K. Yoshimura, V. I. Anisimov, D. Mori, R. Kanno, and R. Ibberson, Nat. Mater. **5**, 471 (2006).
[23] M. Schmidt,W. Ratcliff, P. G. Radaelli, K. Refson, N. M. Harrison, and S. W. Cheong, Phys. Rev. Lett. **92**, 056402 (2004).
[24] Y. Okamoto, S. Niitaka, M. Uchida, T. Waki, M. Takigawa, Y. Nakatsu, A. Sekiyama, S. Suga, R. Arita, and H. Takagi, Phys. Rev. Lett. **101**, 086404 (2008).
[25] P. Blaha, K. Schwarz, G. K. H. Madsen, D. Kvasnicka, and J. Luitz, WIEN2K code, http://www.wien2k.at. Electronic structure calculations were carried out in the generalized gradient approximation (GGA) using the full potential augmented plane wave plus local orbitals method. The muffintin sphere radii were 2.50, 1.87, and 1.66 Bohr for Cs, W, and O, respectively, the number of plane waves was restricted by $R_{MT}k_{max}$ = 7 and the irreducible Brillouin zone was sampled by 726 *k*-points (high temperature phase) and $R_{MT}k_{max}$ = 6 and 100 *k*-points (low temperature phase). W was set as spin up. Spin-orbit coupling was included.
[26] J. Kunes, T. Jeong, and W. E. Pickett, Phys. Rev. B **70**, 174510 (2004).
[27] S. Satpathy, and R. M. Martin, Phys. Rev. B **36**, 7269 (1987).
[28] D. J. Singh, P. Blaha, K. Schwarz, and I. I. Mazin, Phys. Rev. B **60**, 16359 (1999).
[29] Z. Hiroi, S. Yonezawa, Y. Nagao, and J. Yamaura, Phys. Rev. B **76**, 014523 (2007).

Figure Captions

FIG. 1 (color online). Temperature dependence of (a) electrical resistivity, (b) magnetic susceptibility and (c) specific-heat divided by temperature of CsW_2O_6. $C/T(T)$ data is plotted with the fit (solid line) consist of Einstein phonon (broken line) and two Debye phonons (dotted line) as described in ref. [16]. Inset: (a) Arrhenius plot ($\ln\rho(T)$ vs T^{-1}) of CsW_2O_6. (b) Enlarged regions of magnetic susceptibility showing the hysteresis associated with a first order transition. (c) Comparison of $C/T(T)$ between $CsTaWO_6$ (solid line) from ref. [15] and CsW_2O_6 (dots).

FIG. 2 (color online). (a) Portion of the Rietveld fit of the synchrotron X-ray powder diffraction pattern for CsW_2O_6 at 100 K. The triangles mark the superlattice reflections. The inset shows the Rietveld fit of the neutron powder diffraction data at 100 K. (b) The temperature dependence of lattice constants and the integrated intensities of superlattice peak with index (111) in synchrotron X-ray data. The solid lines are guides for the eyes. (c) Electron diffraction pattern for CsW_2O_6 at 100 K with the incident beam parallel to the [110] cubic zone axis. The spots pointed by arrows violate the extinction rules for the F centering of cubic unit cell.

FIG. 3 (color online). (a) WO_6 network at 100 K showing the formation of one-dimensional chains. (b) The relation between cubic cell and orthorhombic cell. (c) W networks on Kagome lattice at 100 K, where W-W bonds with different lengths are shown differently.

FIG. 4 (color online). Electronic density of states (DOS) of CsW_2O_6 at 300 K (dotted line) and 100 K (solid line) as a function of energy in eV. The Fermi energy (E_F) is at 0.

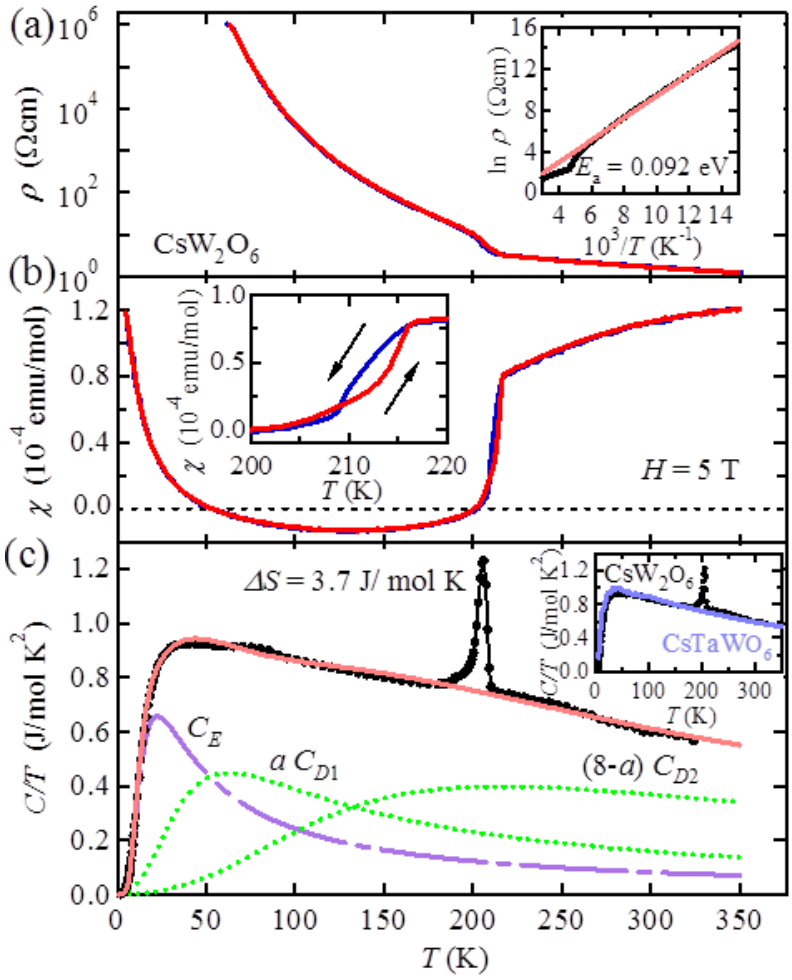
(a)
(b)
(c)
ρ (Ωcm)
CsW2O6
ln ρ (Ωcm)
Ea = 0.092 eV
10^3/T (K^-1)
χ (10^-4 emu/mol)
H = 5 T
T (K)
ΔS = 3.7 J/ mol K
C/T (J/mol K^2)
CE
a CD1
(8-a) CD2
CsTaWO6

Fig. 1

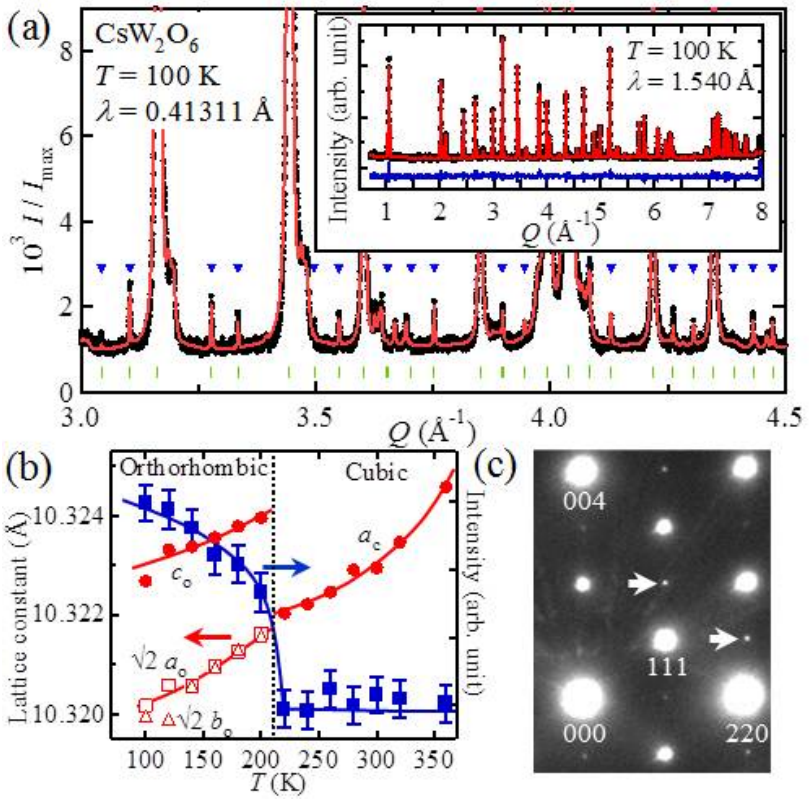
(a)
CsW_2O_6
T = 100 K
λ = 0.41311 Å
10^3 I / I_{max}
Q (Å^{-1})
T = 100 K
λ = 1.540 Å
Intensity (arb. unit)
Q (Å^{-1})
(b)
Orthorhombic
Cubic
a_c
c_o
$\sqrt{2}$ a_o
$\sqrt{2}$ b_o
Lattice constant (Å)
Intensity (arb. unit)
T (K)
(c)
004
111
000
220

Fig. 2

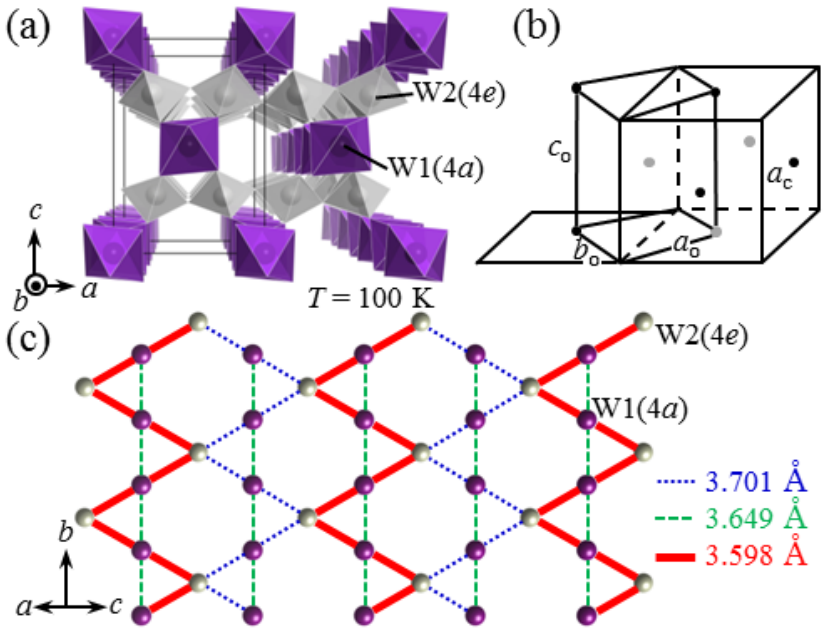
(a)
W2(4e)
W1(4a)
c
b
a
T = 100 K
(b)
c_o
a_c
b_o
a_o
(c)
W2(4e)
W1(4a)
3.701 Å
3.649 Å
3.598 Å
b
a
c

Fig. 3

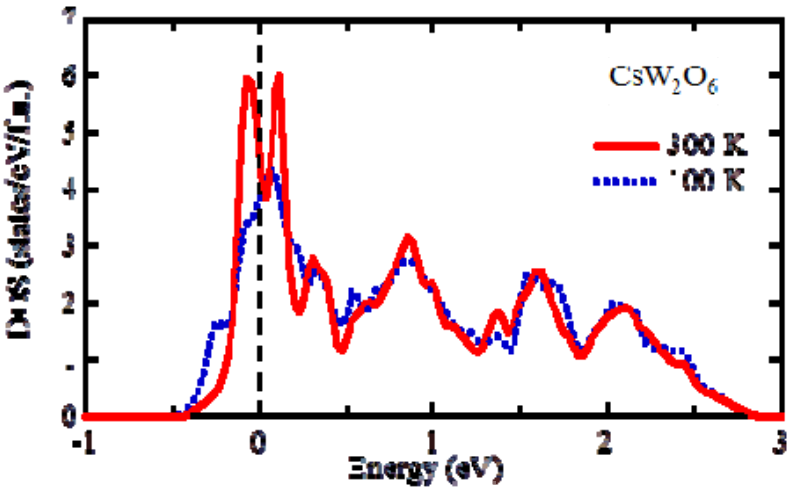

Fig. 4